

Atmospheric-Pressure Microwave Plasma Torch for CVD Technology of Diamond Synthesis

K. F. Sergeichev^{a,*}, N. A. Lukina^a, and N. R. Arutyunyan^{a, b}

^a Prokhorov General Physics Institute of the Russian Academy of Sciences, Moscow, 119991 Russia

^b National Research Nuclear University “MEPhI”, Moscow, 115409 Russia

*e-mail: k-sergeichev@yandex.ru

Received November 19, 2018; revised December 12, 2018; accepted December 20, 2018

Abstract—An electrodeless microwave jet plasma source is considered, and its various applications in the technology of chemical vapor deposition of diamond films and dimension increasing of small diamond single crystals synthesized at high pressures and temperatures are discussed. The plasma jet is ignited in an atmospheric-pressure gas (argon) flow with hydrogen and methane additives. The operation of the microwave jet reactor is described, and the plasma characteristics measured using emission spectroscopy are presented. The brightly glowing atmospheric-pressure plasma jet is ignited and stably burns at a microwave power of ≤ 1 kW supplied from a microwave oven magnetron. The specific microwave power density absorbed by the compact plasma jet ($\leq 10^4$ W/cm³) is comparable with that absorbed by a dc arc. The growth rate of the polycrystalline diamond layer amounts to 40 $\mu\text{m/h}$. The process of film deposition on the substrate can be controlled by scanning the substrate surface with the jet.

DOI: 10.1134/S1063780X19060096

1. INTRODUCTION

Synthesis of diamonds by means of chemical vapor deposition (CVD) on solid surfaces [1, 2] proceeds via chemical reactions occurring in a gaseous medium and involving carbon-containing precursor molecules. The reactions are activated using various thermal methods: hot filament [3], oxyacetylene torch [4], plasma of dc arc discharge in a gas flow [5, 6], plasma of RF [7] and microwave [8–11] discharges, and plasma induced by a CO₂ laser beam [12]. The precursor gases (CH₄ and C₂H₂ hydrocarbons or vapors of organic liquids) excited in the reactive medium are mixed with hydrogen (H₂), the atoms of which remove nondiamond carbon phases from the surface and return them to the gaseous medium. The formation of the diamond phase of carbon on the substrate surface proceeds at temperatures of $700^\circ\text{C} \leq T_s \leq 1000^\circ\text{C}$.

At present, commercial microwave plasma-assisted CVD (MPACVD) reactors, such as the AX 6500 reactor (SEKI Diamond company, www.sekidiamond.com) [9] with a frequency of 2.45 GHz and continuous microwave power of up to 6 kW, as well as the Russian ARDIS reactor [10], the reactor chamber of which is better matched to the waveguide transmission line compared to that of the AX 6500 reactor, are widely used to produce diamond films. Other types of reactors also have received wide application (see review [8]). In those reactors, electrodeless discharge in a gaseous medium at a sub-atmospheric-pressure

from 7×10^3 to 3×10^4 Pa is ignited by microwave radiation. The TEM mode of the coaxial line excites oscillations in the radial line formed by the walls of the axisymmetric chamber and a coaxial disk, above which there is a cylindrical cavity assisting discharge ignition. Plasma looks like a hemispherical cloud with a diameter of $\sim 6 \text{ cm} \sim \lambda/2$, where λ is the microwave wavelength.

The diamond film is deposited on silicon substrates with a diameter of more than 2 inches, which are fixed on molybdenum disks installed below the plasma cloud in the center of a cooled copper disk. The microwave power used in such systems provides deposition of a polycrystalline diamond film on the substrates with a growth rate of 1–10 $\mu\text{m/h}$. The temperature of the substrates heated by the discharge plasma is maintained in the range of 700–1000°C

Unlike other types of discharges, the plasma produced in an electrodeless microwave discharge makes it possible to grow polycrystalline and single-crystal diamond films of high purity. This is due to the absence of impurities in hydrocarbon plasma, which are inherent in plasmas of electrode discharges (hot filament, arc and glow discharges, etc.), because they are always contaminated by the evaporated electrode material.

In this study, we propose to use another type of MPACVD source in which plasma is generated in an atmospheric-pressure gas (argon) jet with additives of

hydrogen and methane. The microwave torch is well known in optical emission spectroscopy (OES) as a compact brightly glowing source of electrodeless plasma [13–15], which is convenient for the excitation and analysis of gaseous media. Due to its small volume, the atmospheric-pressure jet burns stably at a relatively low microwave power of ≤ 1 kW, which can be provided by microwave oven magnetrons. The specific microwave power density absorbed by the compact self-compressed plasma jet ($\leq 10^4$ W/cm³) is comparable to the specific power density absorbed by a dc arc.

The goal of our experiments was to demonstrate the possibility of using a microwave plasma jet for MPACVD synthesis of polycrystalline diamond films on a substrate with an area of ≤ 1 cm². The plasma jet can also be used to increase the thickness of diamond single crystals synthesized by high-pressure high-temperature (HPHT) technique and, probably, to improve the shape of diamond crystals and splice them. The parameters of the microwave plasma jet, such as the electron density and the gas and electron temperatures, were measured. The experimental results on polycrystalline and nanocrystalline diamond film deposition and epitaxial surface growth of diamond single crystals obtained using the HPHT technique are presented.

2. EXPERIMENTAL SETUP

Samsung OM 75 P(31) magnetron 1 (Fig. 1) with a frequency of 2.45 GHz (wavelength of 12.24 cm) and power of 900 W operating in the continuous generation mode was used as the microwave plasma jet energy source. The dominant TE₁₀ mode is excited in rectangular waveguide 2 and then converted into the TEM mode of coaxial waveguide 3. The central conductor of the coaxial waveguide is copper tube 4 with an outer diameter of 6 mm, which has a narrow end with a 1.5-mm-diameter nozzle. Plasma-forming gas (argon) jet 5, flowing out of the nozzle with a flow rate of 3–5 slm at a pressure of $p > 1$ atm, is ionized by the microwave field to form a low-temperature plasma. The plasma jet is separated from the nozzle by the fast outflowing gas, whose velocity (~ 30 – 50 m/s) is higher than the propagation velocity of the ionization front along the gas jet toward the nozzle. The microwave power is transmitted from a coaxial waveguide to the plasma jet due to capacitive coupling between the plasma jet and the coaxial waveguide end. This is the main difference of the microwave torch coupling from that of an RF inductively coupled plasma (ICP) torch [16].

The brightly glowing core of the plasma jet with a diameter of ~ 0.2 cm and length of $\sim \lambda/4 \approx 3$ cm in the microwave discharge region (Fig. 2) contains chemically active atoms and radicals moving toward the substrate with high velocities. Waveguide piston 6 is used to match the impedances of the waveguide mode

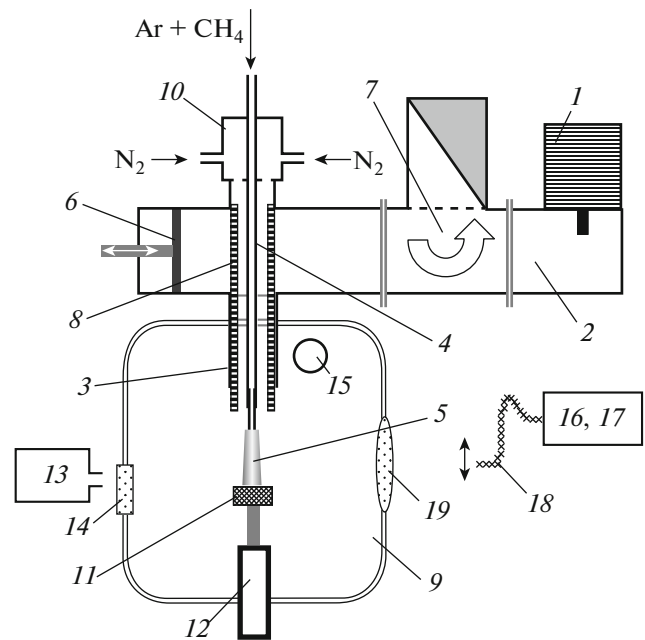


Fig. 1. Experimental arrangement: (1) OM 75 P(31) magnetron, (2) 45×90 -mm rectangular waveguide, (3) coaxial waveguide, (4) central conductor, (5) plasma jet, (6) tuning piston, (7) circulator, (8) quartz tube, (9) reactor chamber, (10) gas mixer, (11) substrate holder, (12) moveable rod, (13) Promin-M1 pyrometer, (14) quartz window, (15) exhaust gas hole, (16) FSD-8 spectrometer, (17) AvaSpec-3648-USB2 spectrometer, (18) optical fiber, and (19) focusing lens.

transducer and plasma jet 5. Before jet ignition, the magnetron is protected from the reflected wave by a water-cooled VFV2-42 waveguide circulator 7, which directs the reflected power onto the absorbing load. Coaxial waveguide 3 is coupled to hollow waveguide 2 by central conductor 4. Radio transparent tube 8, installed instead of the lack part of shield 3, separates waveguide space 2, filled with atmospheric-pressure air, from the vacuum-sealed region of reactor 9, where the coaxial plasma jet operates. The plasma jet is formed in monatomic argon. To synthesize diamond, a hydrogen–methane mixture (methane as a carrier of carbon atoms) is added to argon. Methane is introduced into the argon jet through mixer 10. Hydrogen is supplied through the space between conductor 4 and quartz tube 8. The diamond film is deposited on a substrate, which is placed under the jet on water-cooled holder 11 and can be moved vertically with the help of moveable rod 12. Since the substrate is heated to the working temperature (750 – 1000°C) by the plasma jet, the temperature of the substrate surface can be controlled by varying the distance between the substrate and the plasma jet end. The substrate is placed outside the region of active microwave power absorption by the plasma jet, which makes it possible to locally deposit diamond films on substrates of dif-



Fig. 2. (Color online) Photograph of a microwave plasma jet.

ferent shapes and sizes and scan the substrates by the jet along arbitrary trajectories.

The substrate surface temperature is monitored using optical pyrometer *13* through quartz window *14*. The pyrometer operation is based on the equalizing brightnesses of the object image and the pyrometric lamp filament. In the given temperature range, the accuracy of temperature measurements is $\sim 20^\circ\text{C}$.

The area of diamond film deposition is $\sim 1\text{ cm}^2$, which is much larger than the cross-sectional area of the plasma jet core ($\approx 0.1\text{ cm}^2$). This is due to the gas-dynamic properties of the plasma jet, which spreads out radially over the substrate surface, which is a barrier for the gas flow. Hydrocarbon species produced in the microwave field are transported to the substrate by the gas jet. During plasma jet operation, gas pressure equilibrium in the reactor chamber *9* is established due to the natural balance between the inflow of the gas mixture and its outflow through exhaust air hole *15* due to a slight excess of the gas pressure in the chamber over the atmospheric pressure. The gas flow rates were measured using float-type flowmeters installed at the outlets of DINFLOW N10-3-30 gas cylinder reducers. The hydrogen flow rate was measured with a ZYIA Instr. Co. flowmeter. In these experiments, the argon and hydrogen flow rates were varied in the ranges of 2.5–5 slm (standard liter per minute) and 0.5–1 slm, respectively. In these experiments, the methane content was from 1 to 4% relative

to the hydrogen concentration. Varying the gas mixture composition, we could change the structure of polycrystalline diamond films from a microcrystalline structure to nanocrystalline and ultrananocrystalline structures.

The parameters of the discharge plasma were estimated using spectral instruments with different resolutions in the wavelength range of 300–1000 nm: FSD-8 spectrometer *16* with a resolution of 10 nm and an AvaSpec-3648-USB2 spectrometer with a resolution of 0.3 nm. The FSD-8 spectrometer was used to monitor the burning mode of the plasma jet. The electron density and gas temperature of the plasma jet in the course of CVD diamond synthesis were determined from the contours of the Balmer lines of atomic hydrogen and the rotational spectrum of the C_2 molecule (the Swan spectral band of the 0–0 vibrational transition). To this end, a spectrometer with a high resolution of $\sim 0.04\text{ nm}$ was used. The image of the plasma jet was projected onto the input end of a quartz fiber, the other end of which was installed near the entrance slit of the spectrometer. Moving the end of the fiber, we could measure the spatial distributions of the plasma jet parameters with a spatial resolution determined by the fiber diameter (0.3 mm for the FSD-8 spectrometer).

3. IGNITION OF THE PLASMA JET AND DESCRIPTION OF ITS PROPERTIES

The ignition of the discharge and its transition into the steady-state operating mode are carried out in three successive steps. To expel air from the chamber, the latter is blown off with nitrogen at a pressure higher than atmospheric. Then, argon is supplied through the nozzle and, after the microwave generator is switched on, gas discharge in the jet is ignited. In the initial stage, in order to avoid explosion of flammable gases when they are mixed with residual oxygen, nitrogen serves as a flegmatizing agent. Then, after nitrogen flow is cut off, hydrogen is supplied, which gradually replaces nitrogen in the chamber. Finally, as nitrogen is being expelled by hydrogen, methane–argon, gas balance is established, i.e., the plasma jet reaches a steady-state burning mode. The partial concentrations of the gas components in the steady-state mode are proportional to the gas flow rates: $\text{Ar} : \text{H}_2 : \text{CH}_4 = 4.5 : 1.0 : (0.02\text{--}0.04)\text{ slm}$.

The cross-section-averaged emission spectra measured by the FSD-8 spectrometer with a low resolution in different stages of the discharge are shown in Fig. 3. When the plasma jet operates in nitrogen (Fig. 3a), bright argon lines are observed in the blue region of the spectrum, which are not resolved in detail by the FSD-8 spectrometer. In this case, no substantial excitation of nitrogen was observed. After the nitrogen flow is cut off and replaced with hydrogen (Fig. 3b), the argon lines disappear and the 654-nm

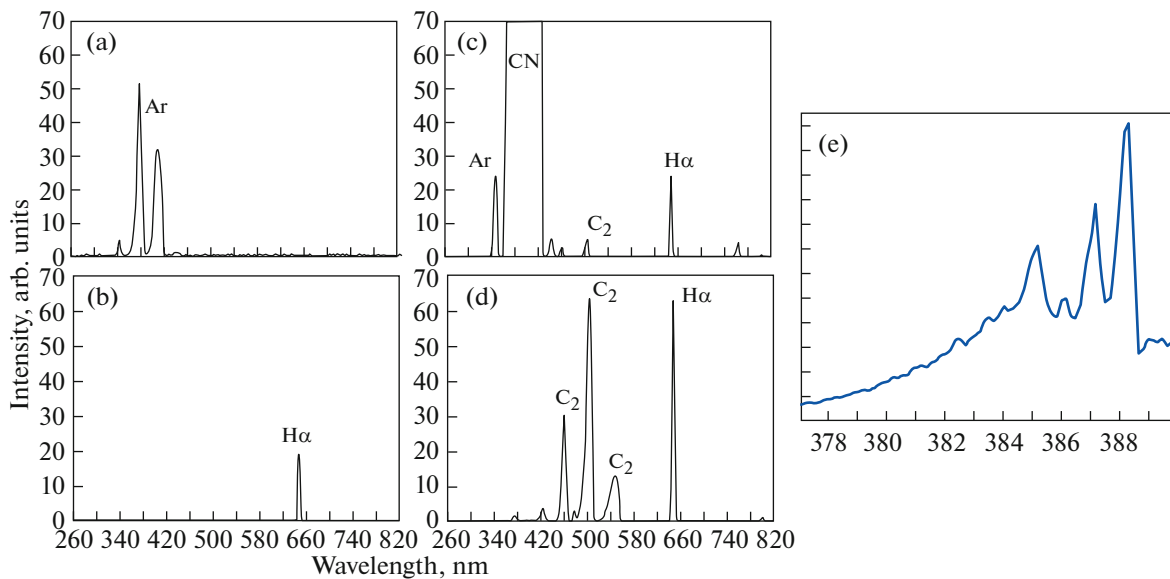


Fig. 3. (Color online) Optical emission spectra of the microwave plasma jet in different stages of the discharge measured with the FSD-8 spectrometer: (a) jet ignition in the argon flowing out into the nitrogen atmosphere, (b) replacement of nitrogen with hydrogen, (c) addition of methane to argon, (d) jet plasma spectrum measured in the steady-state mode, and (e) spectrum of CN molecules measured with the “AvaSpec” spectrometer.

H_{α} line of hydrogen arises. Adding methane to the gas mixture in the presence of nitrogen (Fig. 3c) is accompanied by the appearance of strong emission near the wavelength of 380 nm, which increases for up to 8 min, as well as a less intense emission near the wavelengths of 400, 516, and 654 nm. The emission spectrum near 380 nm, measured by using the AvaSpec spectrometer, was identified as a 385- to 388-nm CN molecular band with a tail on the violet side [17]. In this spectral region, the relatively weak ${}^1\Pi \rightarrow {}^1\Pi$ C_2 bands (with heads at 382.5 and 385.2 nm and tails on the violet side) can additionally overlap with the ${}^2\Sigma \rightarrow {}^2\Pi$ CH bands (with heads at 362.8 and 388.9 nm and tails on the red side). As methane is fed, the H_{α} line intensity somewhat decreases and the H_{β} 486-nm line and green emission of C_2 molecules (the ${}^3\Pi_u$ transition with a head at 516 nm) appear, the intensities of which increase simultaneously and reach their maxima about 15 min after the methane flow is switched on. In the steady-state mode, the spectra are characterized by the intense H_{α} and H_{β} hydrogen lines, as well as by the bands of C_2 molecules and CH radicals (the ${}^2\Delta-{}^2\Pi$ transition with a head at 431 nm). The intensity of the CN band reaches its minimum value only after 40 min, when nitrogen is completely replaced with hydrogen.

The processes occurring in different stages of the microwave jet burning is qualitatively described as follows. When the discharge is ignited, the ambient nitrogen does not interact with the plasma jet; thereby, it prevents transverse arc microwave breakdown between the nozzle and the edge of the outer coaxial electrode

of the plasma torch. Note that, in a pure argon atmosphere, the plasma jet is not formed due to the transverse breakdown between the electrodes. In the nitrogen atmosphere, the bands of the second positive system of nitrogen, as well as argon lines, are so weak that the FSD-8 spectrometer does not fix them. When hydrogen is fed, it begins to react with argon, but nitrogen remains neutral. The energy of excited argon atoms in the plasma jet is mainly spent on the dissociation of hydrogen and excitation of its atoms. As a result, the intensity of argon emission decreases and the intense H_{α} line appears in the emission spectrum. When methane is introduced in the discharge together with argon, nitrogen actively interacts with methane, producing new molecular species (CN, C_2 , and C_xH_y hydrocarbons), and the energy of excited argon atoms is redistributed between hydrogen and methane. In the steady-state mode of the jet burning, weak emission of CN molecules remains after nitrogen is completely replaced with hydrogen, which indicates the presence of residual nitrogen in the chamber. We note that nitrogen can also be present as an impurity in the technical gases used in these experiments.

The dynamics of the main components of the emission spectrum during the steady-state discharge establishment is shown in Fig. 4. Up to 6 min after microwave discharge ignition, the intensities of all main spectral components grow while nitrogen is gradually replaced with hydrogen. Then, the argon emission intensity decreases exponentially with time, while the emission intensities of atomic hydrogen and C_2 dimer are stabilized. The steady-state discharge

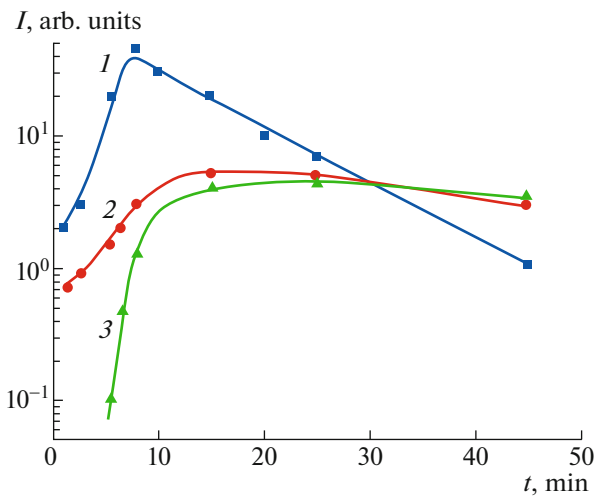


Fig. 4. (Color online) Dynamics of the main components of the discharge emission spectrum (from ignition to steady-state mode): (1) Ar, (2) H_{α} , and (3) C_2 band (head of the ${}^3\Pi_u$ transition, 516 nm). The flow rates of the working gases are Ar : H_2 : CH_4 = 5 : 1 : 0.06 slm.

mode is reached in 40 min, when almost no nitrogen remains in the chamber and the gas composition balance in the jet and in the chamber volume is reached.

The measurements with the FSD-8 spectrometer have shown that, during deposition of diamond films, the intensities of the H_{α} line and the C_2 molecular band are comparable.

Hydrogen plays an important role in the diamond formation process. The presence of hydrogen ensures the priority growth of the sp^3 diamond phase compared to the graphite phase. This is because atomic

hydrogen quickly gasifies graphite, returning it into the gaseous medium in the form of hydrocarbon compounds, practically not affecting the synthesized diamond.

The optimal hydrogen content in argon was determined experimentally by varying the hydrogen flow rate at two fixed argon flow rates (3 and 5 slm) and a fixed microwave power (Fig. 5a). The H_{α} line intensity, which is proportional to the concentration of excited atoms, depends nonmonotonically on the hydrogen flow rate. It grows as the hydrogen flow rate increases to ~ 0.5 slm and begins to decrease when the hydrogen flow rate exceeds 1 slm. The lower the argon flow rate, the faster the decrease in the H_{α} line intensity (see Fig. 5a; curves 1, 2). Both dependences have maxima at a flow rate of ~ 1 slm, which allows us to conclude that the content of hydrogen atoms in plasma is optimal at this flow rate. The decline of the dependences at higher hydrogen flow rates is apparently due to the energy stored in metastable levels of argon atoms in the plasma jet being insufficient for the total dissociation of molecular hydrogen. We note that an increase in the argon flow rate intensifies generation of atomic hydrogen, which is consistent with the assumption on the key role of metastable states of argon atoms in hydrogen dissociation.

The ratio between the methane and hydrogen flow rates that is optimal for the growth of a diamond film was determined from the dependence of the C_2 band intensity on the methane flow rate. The growth rate of the diamond film reaches its maximum value when the intensity of the C_2 band becomes close to the H_{α} line intensity (being measured with the low-resolution FSD-8 spectrometer) (Fig. 5b). The measurements were performed on the plasma jet axis at $z = 1.5$ cm. In this experiment, the ratio between the argon and

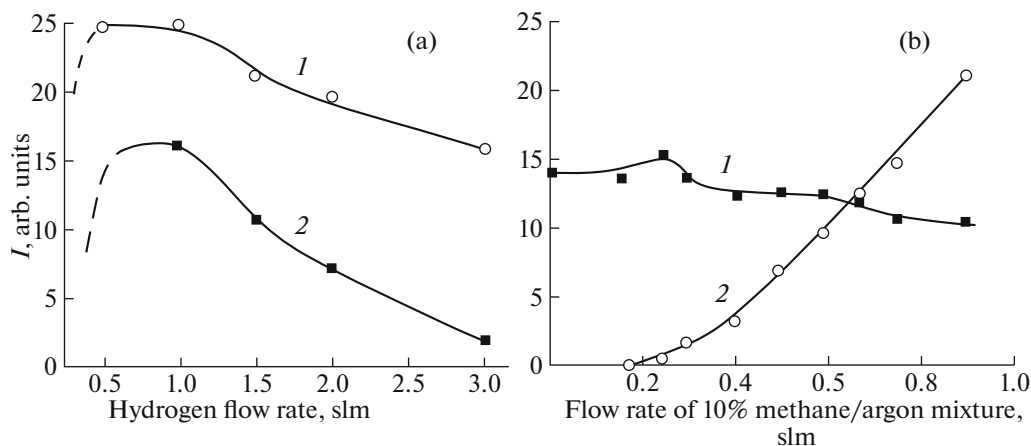


Fig. 5. Intensities of the H_{α} line of atomic hydrogen (654 nm) and C_2 dimer Swan band (516 nm) as functions of the gas flow rates: (a) H_{α} intensity vs. hydrogen flow rate for two different argon flow rates: (1) 5 and (2) 3 slm; (b) intensities of the (1) H_{α} line and (2) C_2 band vs. flow rate of methane–argon mixture at a constant ratio of the argon and hydrogen flow rates, Ar : H_2 = 4.5 : 1 slm.

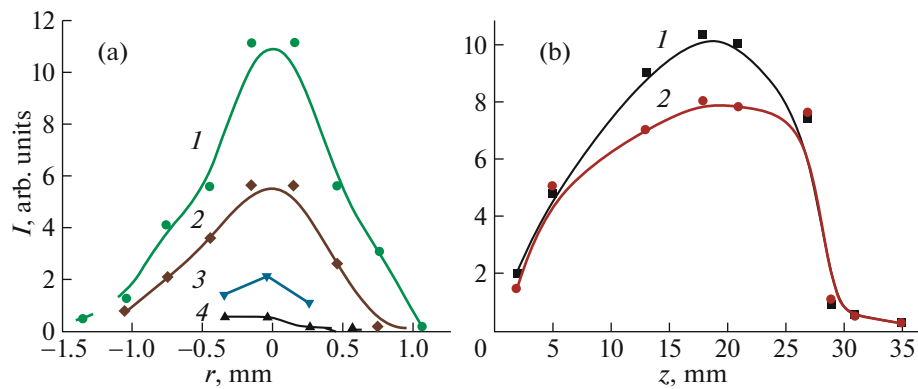


Fig. 6. (Color online) Intensity profiles of atomic spectral lines and molecular spectral bands used to determine the parameters of the steady-state microwave plasma jet: (a) transverse profiles of the emission intensities of (1) C_2 , (2) H_α , (3) Ar (763.5 nm), and (4) CH; (b) longitudinal profiles of the emission intensities of (1) C_2 molecular band and (2) H_α line. The flow rates of the working gases are Ar : H_2 : CH_4 = 5 : 1 : 0.06 slm.

hydrogen flow rates was kept constant (Ar : H_2 = 4.5 : 1 slm), while the methane content in hydrogen was varied by varying the methane flow rate from 0 to 0.09 slm. It was ascertained that 6% content of methane in hydrogen is optimal for the growth of a diamond film.

Figure 6 shows the transverse and longitudinal profiles of the intensities (in arbitrary units) of the lines and bands of the main spectral components observed in the steady-state mode of diamond synthesis. Figure 6a shows the intensity profiles of the C_2 and CH spectral bands and H_α and Ar lines were measured with the FSD-8 spectrometer across the jet at a distance of 1.5 cm from the nozzle. Figure 6b shows the longitudinal profiles (along the jet axis) of the main spectral components (C_2 band and H_α line) measured in the course of diamond film growth. The distance z is counted from the nozzle.

In the steady-state mode of diamond film deposition, the H_α line and C_2 band are the brightest in the microwave spectrum of the plasma jet. The degree of hydrogen dissociation was qualitatively estimated from the intensity of the H_α line, while the plasma electron density was determined from the width of the line profile. The emissions of the C_2 и CH bands (431 nm) indicate that methane is decomposed with the formation of the C_2 molecules and, apparently, CH_3 (methyl) radicals, which are often considered to be precursors of the diamond formation. The emission of the CH_3 band in the long-wavelength part of the IR spectrum (near 16.2 μm) was not detected, because it was beyond the spectral ranges of the spectrometers.

Since the discharge plasma is inhomogeneous, the diamond film growth can be affected by both the plasma composition and the substrate temperature, which depend on the substrate position under the jet. In order to provide optimal conditions for the dia-

mond growth, the gas flow rates and the magnetron power should be thoroughly monitored.

Thus, the diameter of the plasma core is in the range of $2\text{ mm} < 2r < 3\text{ mm}$, while its length along the axis is $\geq 30\text{ mm}$. Optimal conditions for the growth of the diamond film take place in the region where the C_2 and H_α intensities are maximal (according to FSD-8 measurements) and comparable in order of magnitude (Fig. 6b). The optimal distance from the substrate to the nozzle was $z \leq 25\text{ mm}$.

4. PARAMETERS OF THE ATMOSPHERIC-PRESSURE MICROWAVE PLASMA JET. DISCUSSION OF THE MEASUREMENT RESULTS

The gas temperature T_g in the plasma jet has a strong effect on the processes of diamond growth [18]. The best estimate of the gas temperature can be obtained from the rotational temperatures determined from the rotational spectrum of the 0–0 vibrational band of the $d^3\Pi_g - a^3\Pi_u$ electron transition of the C_2 radical [19, 20]. According to modern concepts [21], during the diamond lattice formation, the concentration of C_2 radicals exceeds the CH_3 concentration. The problem of measuring the gas temperature in a non-equilibrium plasma was considered in [22]. During CVD synthesis of a polycrystalline diamond film, the temperature was determined by measuring the rotational spectra of the C_2 radical in the lower part of the plasma jet near the substrate surface [18]. The rotational temperature determined from the upper level emission was found to be $\sim 4000\text{ K}$. According to [22], in a nonequilibrium plasma, the rotational spectral density of a diatomic molecule should not necessarily be in equilibrium with the gas temperature determined by the translational molecule motion. Thermal equilibrium is more typical of a low-pressure low-density

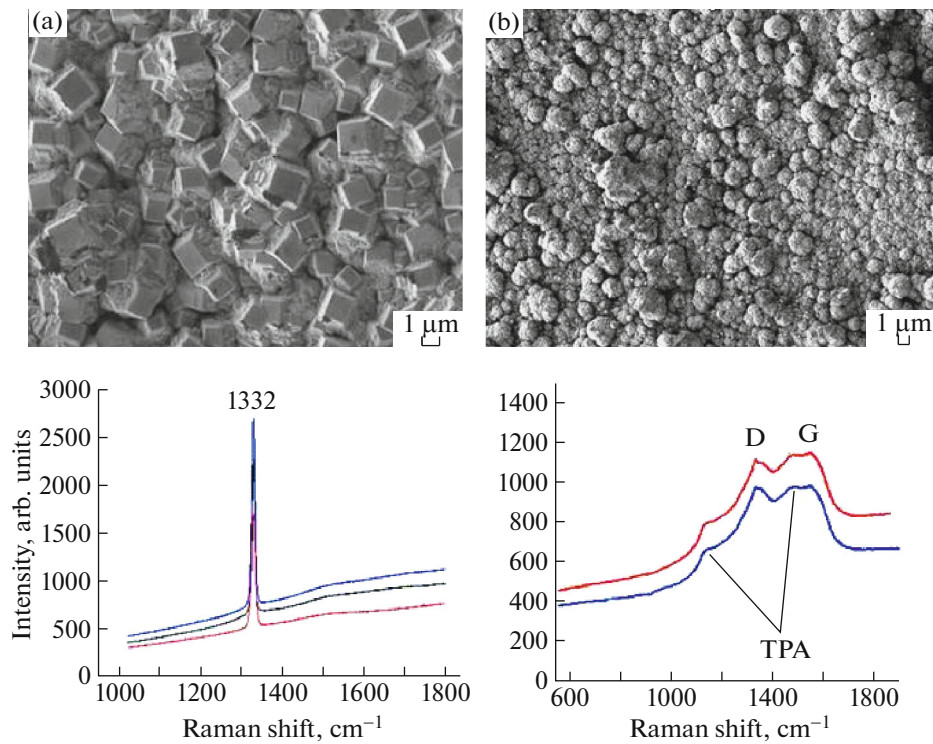


Fig. 7. (Color online) Photographs and the corresponding Raman spectra of the deposited diamond films: (a) microcrystalline film deposited on a molybdenum substrate and (b) nanocrystalline film deposited on a silicon substrate.

plasma in which no collisions occur during the lifetime of the excited state. In this case, electron impact is the dominant mechanism of excitation. The atmospheric-pressure microwave plasma jet is another limiting case with a high collision frequency and relatively long lifetimes of electronic states. During the lifetime of the electronic state, the excited molecule can undergo several collisions with other gas molecules. These collisions thermalize the potentially nonthermal distribution of the populations of rotational levels before a photon is emitted.

Another important parameter that has a strong effect on the processes of CVD diamond synthesis is the electron temperature. Plasma electron density is usually determined from the Stark broadening of the H_α and H_β hydrogen lines of the Balmer series. However, in [23], it was demonstrated that the electron density n_e and electron temperature T_e of hydrogen plasma can be simultaneously determined using the spectral method based on the analysis of the $n_e(T_e)$ dependences obtained from data on three hydrogen lines (H_α , H_β , and H_γ) measured at a constant value of the Stark broadening, $\Delta\lambda_{1/2} = \text{const}$, used as a parameter. This diagnostic method, called the $n_e(T_e)$ intersection method, made it possible to determine both n_e and T_e from the intersection point of the $n_e(T_e)$ dependences at a microwave power of 600 W. In [23], measurements were performed for a microwave discharge

ignited in an argon flow with a hydrogen admixture at atmospheric pressure under conditions close to those of our experiment. This allowed us to use data of [23] to estimate the mean electron temperature in the microwave plasma jet, which was found to be $T_e \geq 1.5$ eV. The mean electron density determined from the Stark broadening of the H_β line [24] turned out to be $\langle n_e \rangle \approx 4 \times 10^{15} \text{ cm}^{-3}$.

5. DIAMOND FILMS OBTAINED IN THE MODES OF HOMOEPITAXIAL, NANOCRYSTALLINE, AND POLYCRYSTALLINE GROWTH OF DIAMOND IN THE MICROWAVE PLASMA JET

Using an atmospheric-pressure microwave plasma jet, microcrystalline [25, 26] and nanocrystalline films were deposited on silicon [27] and molybdenum substrates (Fig. 7), as well as homoepitaxial deposition of diamond on the HPHT monocrystalline substrates [28] was performed (Fig. 8).

A molybdenum substrate with dimensions of $15 \times 15 \times 2$ mm (Fig. 7a) was preliminarily seeded using a diamond powder suspension in an alcohol–acetone solution. The seeding was performed for 14 min in a cavity irradiated by ultrasound. Then, the substrate was fixed on a moveable holder and installed in the

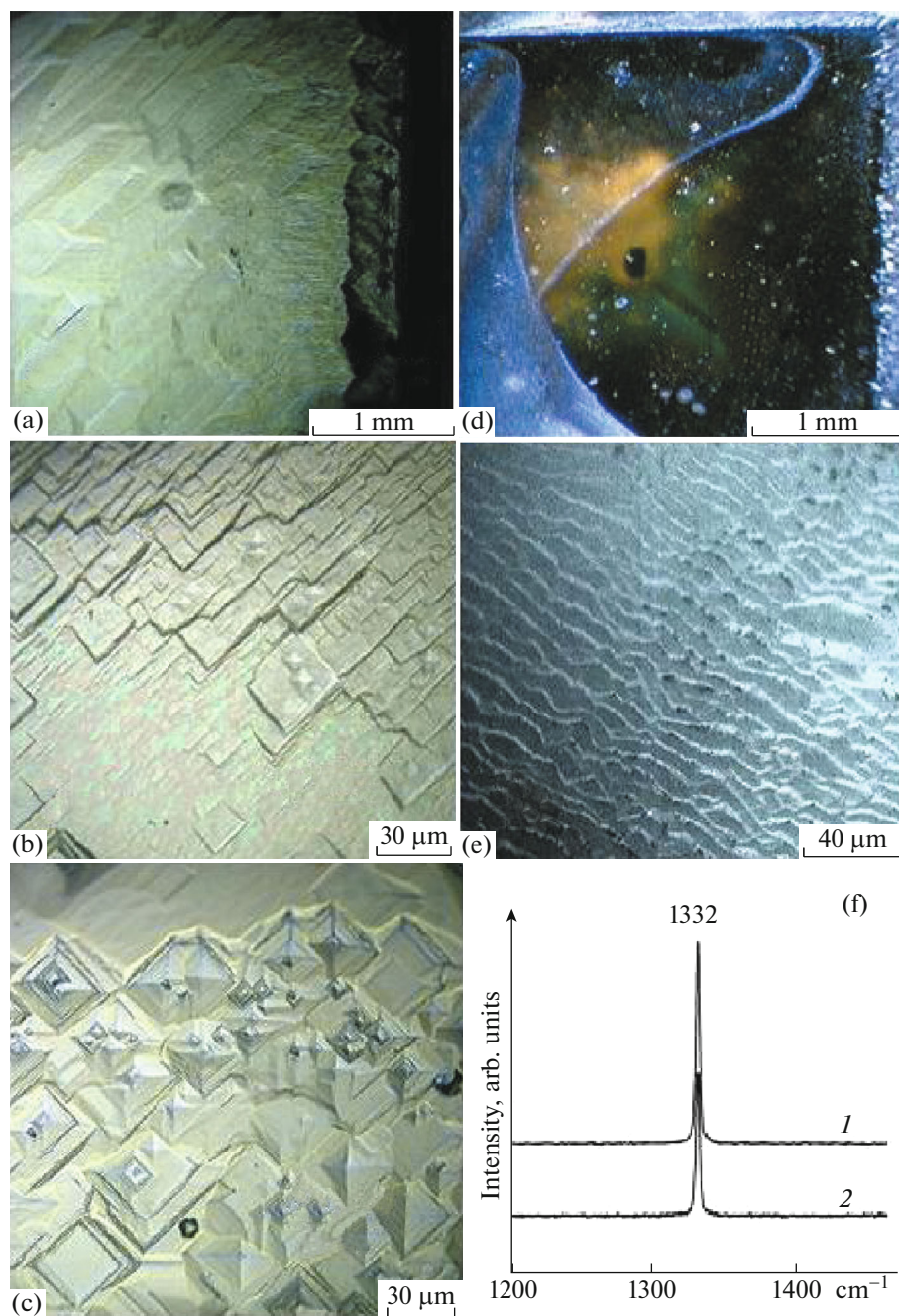


Fig. 8. (Color online) (a, d) Macro- and (b, c, e) microscale images of the surface structure of diamond films grown on HPHT diamond single crystals and (f) Raman spectrum of the grown film with a narrow diamond peak at 1332 cm^{-1} .

reactor chamber under the plasma jet. The diamond deposition was performed at a substrate temperature of $850\text{--}1000^\circ\text{C}$ at a distance of 25 mm from the nozzle. The flow rates of the working gases were $\text{Ar} : \text{H}_2 : \text{CH}_4 = 5 : 1 : 0.01$ slm. The deposition proceeded for 3 h. The mean thickness of the deposited microcrystalline film was $60\ \mu\text{m}$, and the deposition area was ~ 1 cm in diameter. The film consists of microcrystals with (100) orientation and side dimensions of

$\sim 3\text{--}4\ \mu\text{m}$. The Raman spectra of the films are shown below the photographs. A narrow peak at 1332 cm^{-1} corresponding to diamond can be seen in the spectra of the monocrystalline film, which were obtained by laser probing at three different points. The nanocrystalline film (Fig. 7b) was deposited on the polished surface of a $16 \times 16 \times 3\text{-mm}$ silicon substrate. The surface was preliminary seeded for 20 min by using a diamond nanopowder suspension in a cavity irradiated by

ultrasound with a power of 50 W. The deposition was performed at a substrate temperature of $\sim 800^\circ\text{C}$ at a distance of 35 mm from the nozzle. The flow rates of the working gases were $\text{Ar} : \text{H}_2 : \text{CH}_4 = 3 : 0.6 : 0.01$ slm. The deposition time was 4 h. The film is characterized by the “cauliflower” morphology. In the Raman spectra, protrusions typical of D and G nanocrystalline diamond films, as well as of trans-polyacetylene (TPA), are observed.

The homoepitaxial diamond growth experiments with HPHT crystals were performed using samples with dimensions of $4 \times 4 \times 1$ and $4 \times 4 \times 2$ mm. Photographs of the crystals are shown in Figs. 8a and 8d. The morphology of the grown homoepitaxial diamond layers can be seen in Figs. 8b, 8c, and 8e, while the Raman spectrum of the grown layer is shown in Fig. 8f. To retain crystals under the gas jet, they were fixed on molybdenum holders using graphite-based heat-resistant glue.

The homoepitaxial layers were deposited on the faces (100) of HPHT diamond crystals (Fig. 8a) at a distance of 30 mm from the nozzle at a temperature of $900\text{--}1000^\circ\text{C}$. The flow rates of the working gases were $\text{Ar} : \text{H}_2 : \text{CH}_4 = 4.7 : 1 : 0.04$ slm. The deposition time was 3.5 h. The structure of the deposited transparent epitaxial layer is characterized by the presence of typical oriented “steps” (Fig. 8b) and “pyramids” (Fig. 8c). The thickness of the grown layer is $65\ \mu\text{m}$. At a low magnification, the transparent epitaxial diamond layer deposited on the HPHT sample (Fig. 8d) looks like water poured along the top and left edges. The diamond layer grew from the edge to the center, because the jet was displaced from the center of the crystal. During the layer growth, the sample was rotated by 90° about the axis. The deposition was performed at a temperature of $800\text{--}900^\circ\text{C}$. The distance to the nozzle was 30 mm. The flow rates of the working gases were $\text{Ar} : \text{H}_2 : \text{CH}_4 = 5 : 1 : 0.25$ slm. The deposition time was 2 h. The transparent epitaxial diamond film grown on the (100) crystal face has typically oriented growth “steps” with a width of $6\text{--}10\ \mu\text{m}$ and height of $\sim 1\ \mu\text{m}$. The step morphology of the film growth (Fig. 8d) can be due to the oblique orientation of the crystal cut relative to the (100) crystallographic orientation. When the crystal cut is oriented parallel to the (100) crystal surface, the morphology becomes pyramidal (Fig. 8c). The Raman spectra of the grown layers are characterized by the presence of a narrow diamond peak at $1332\ \text{cm}^{-1}$.

6. CONCLUSIONS

A electrodeless microwave discharge freely burning in an argon jet ejected from the torch nozzle has been studied experimentally. The plasma jet has no contact with the metal nozzle, because the ionization wave front propagating along the argon jet toward the nozzle is permanently blown away by the fast gas flow. The

microwave energy is transferred through the gas gap due to the capacitive coupling between the plasma and the coaxial torch. The burning jet is a source of pure plasma. In the plasma jet with a gas temperature of up to 4000 K, the methane and hydrogen admixed to the argon jet form a reactive medium above the substrate in which proper conditions for the diamond growth are created. The substrate is heated to a temperature of $\leq 1000^\circ\text{C}$, which is established due to the heat balance between the substrate and plasma jet. The parameters of the nonequilibrium plasma, such as the plasma density, electron temperature, and gas temperature in the jet, were estimated from the measured emission spectra. It is shown that the diameter of the region on the substrate on which the polycrystalline film was deposited is ≤ 10 mm. According to gas-dynamic laws, after colliding with the substrate, the narrow plasma jet spreads over its surface. The growth rate of the diamond layer amounts to $40\ \mu\text{m/h}$.

The small area of the film deposition can be considered a disadvantage of the microwave plasma jet reactor compared to other types of microwave reactors, which are mainly intended to grow large-area polycrystalline diamond films and plates. However, these reactors are less suitable for the additional homoepitaxial growing-up of synthetic (HPHT) diamond single crystals with dimensions less than 1 cm. In these reactors, the problem of an uneven crystal growth followed by the formation of a polycrystalline “necklace” arises, which limits the growth of a single crystal.

A free microwave plasma jet seems to be more attractive for the dimension increasing and junction of diamond single crystals up to the size that fits the size of film deposition region. The background microwave field near the jet weakly affects the growth of a diamond film, while the directional motion of the plasma jet toward the substrate accelerates its growth.

Substrate surfaces of any shape and size can be processed by scanning them with the microwave plasma jet. Scanning by the plasma jet can also be used to grow diamond single crystals with dimensions larger than the diameter of the spot that can be processed by an immovable plasma jet. This distinguishes the microwave plasma jet from the reactors in which the diamond film is deposited in microwave cavities strictly satisfying the boundary conditions in order for not to disturb the field structure. By scanning the jet, one can deposit curved and profiled polycrystalline diamond coatings, including nanocrystalline coatings, on flat and cylindrical surfaces. This can be used to harden the cutting edges of metal-working tools, in particular, tungsten carbide cutting inserts.

ACKNOWLEDGMENTS

The authors are grateful to A.A. Letunov for his help in measurements of the discharge plasma charac-

teristics and to D.I. Svetogorov for providing us with an HPHT diamond single crystal used in experiments on the epitaxial crystal growth.

FUNDING

This work was supported by the Prokhorov General Physics institute of the Russian Academy of Sciences within the scope of the research program “Fundamentals of plasma, microwave, and beam technologies” (state contract no. 0024-2018-0046).

REFERENCES

1. B. V. Derjaguin, D. V. Fedoseev, V. M. Lukyanovich, B. V. Spitzin, V. A. Ryabov, and A. V. Lavrentyev, *J. Crystal Growth* **2**, 380 (1968).
2. *Diamond Films Handbook*, Ed. By J. Asmussen and D. Reinhard (CRC Press, Boca Raton, FL, 2002).
3. S. Matsumoto, M. Kamo, and N. Setaka, *Jpn. J. Appl. Phys.* **21**, L183 (1982).
4. Y. Matsui, *Jpn. J. Appl. Phys.* **29**, 155 (1990).
5. K. Kurihara, K.-I. Sasaki, and M. Kawarada, *Fujitsu Sci. Tech. J* **25**, 44 (1989).
6. J. M. Olson and M. J. Dawes, *J. Mater. Res.* **11**, 1765 (1996).
7. S. K. Baldwin, T. G. Owano, and C. H. Kruger, *Plasma Chem. Plasma Process.* **14**, 383 (1994).
8. F. Silva, K. Hassouni, X. Bonnin, and A. Gicquel, *J. Phys. Condens. Matter* **21**, 364202 (2009).
9. M. M. Besen, E. Sevillano, and D. K. Smith, US Patent No. 5.501.740, March 26, 1996.
10. V. I. Konov, V. G. Ral'chenko, K. F. Sergeichev, V. B. Khavaev, S. K. Vartapetov, and V. V. Atezhev, RF Patent No. 2299929, Application No. 2005125464, Priority from August 11, 2005.
11. A. P. Bolshakov, V. I. Konov, A. M. Prokhorov, and S. A. Uglov, *Diamond Relat. Mater.* **10**, 1559 (2001).
12. A. L. Vikharev, A. M. Gorbachev, A. V. Kozlov, D. B. Radishev, and A. B. Muchnikov, *Diamond Relat. Mater.* **17**, 1055 (2008).
13. M. C. Garcia, A. Rodero, and A. Sola, *Spectrochim. Acta B* **55**, 1733 (2000).
14. D. V. Vlasov, K. F. Sergeichev, and I. A. Sychev, *Plasma Phys. Rep.* **28**, 444 (2002).
15. Y. Mitsuda, T. Yoshida, and K. Akashi, *Rev. Sci. Instrum.* **60**, 249 (1989).
16. E. A. H. Timmermans, I. A. J. Thomas, J. Jonkers, E. Hartgers, J. A. M. van der Mullen, and D. C. Schram, *Fresenius J. Anal. Chem* **362**, 440 (1998).
17. https://physics.nist.gov/PhysRefData/ASD/lines_form.html.
18. A. A. Letunov, N. N. Skvortsova, N. A. Lukina, K. F. Sergeichev, and N. S. Petrovskii, *VIII International Symposium on Theoretical and Applied Plasma Chemistry, Ivanovo, 2018*, Book of Abstracts.
19. S. Pellerin, K. Musiol, O. Motret, B. Pokrzywka, and J. Chapelle, *J. Phys. D* **29**, 2850 (1996).
20. E. V. Bushuev, V. Yu. Yurov, A. P. Bolshakov, V. G. Ralchenko, A. A. Khomich, I. A. Antonova, E. E. Ashkinazi, V. A. Shershulin, V. P. Pashinin, and V. I. Konov, *Diamond Relat. Mater.* **72**, 61 (2017).
21. C. Rond, S. Hamann, M. Wartel, G. Lombardi, A. Gicquel, and J. Röpcke, *J. Appl. Phys.* **116**, 093301 (2014).
22. P. J. Bruggeman, N. Sadeghi, D. C. Schram, and V. Lins, *Plasma Sources Sci. Technol.* **23**, 023001 (2014).
23. J. Torres, J. M. Palomares, A. Sola, J. J. A. M. van der Mullen, and A. Gamero, *J. Phys. D* **40**, 5929 (2007).
24. H. Griem, *Plasma Spectroscopy* (McGraw-Hill, New York, 1964).
25. K. F. Sergeichev, N. A. Lukina, A. P. Bol'shakov, V. G. Ral'chenko, N. R. Arutyunyan, S. N. Bokova, and V. I. Konov, *Prikl. Fiz.*, No. 6, 39 (2008).
26. K. F. Sergeichev, N. A. Lukina, A. P. Bolshakov, V. G. Ralchenko, N. R. Arutyunyan, I. I. Vlasov, *Plasma Phys. Rep.* **36**, 1272 (2010).
27. A. M. Anpilov, N. R. Arutyunyan, E. M. Barkhudarov, I. V. Belashov, A. P. Bolshakov, M. A. Borisenko, V. A. Ivanov, I. A. Kossyi, N. A. Lukina, Ph. O. Milovich, V. S. Sedov, M. A. Abakumov, and K. F. Sergeichev, *J. Phys. Conf. Ser.* **1094**, 012030 (2018).
28. K. F. Sergeichev and N. A. Lukina, *Plasma Phys. Rep.* **37**, 1224 (2011).

Translated by I. Grishina